

Roles of RMP-induced Changes of Radial Electric Fields in ELM Suppression

L. Shi, S. Taimourzadeh, I. Holod, Z. Lin, University of California, Irvine, USA
(Email: zhihongl@uci.edu)

N. Ferraro, R. Nazikian, Princeton Plasma Physics Laboratory, Princeton, USA
H. Y. Wang, J. Y. Fu, Fusion Simulation Center, Peking University, Beijing, China
D. Spong, Oak Ridge National Laboratory, Oak Ridge, TN 37831, USA

Abstract.

Gyrokinetic GTC simulations of DIII-D tokamak with axisymmetric equilibrium show that the reduction in the radial electric field shear at the top of the pedestal during edge localized mode (ELM) suppression with the $n = 2$ resonant magnetic perturbations (RMPs) leads to enhanced drift-wave turbulence and extended turbulence spreading to the top of the pedestal relative to ELMing plasmas with similar RMP and pedestal parameters. The simulated turbulent transport at the top of the pedestal in ELM suppressed conditions is consistent with experimental observations of enhanced turbulence at the top of the pedestal during ELM suppression by the RMPs. These results suggest that enhanced drift-wave turbulence due to reduced ExB shear at the pedestal top can contribute to the additional transport required to prevent the pedestal growing to a width that is unstable to ELMs. Furthermore, GTC simulations of neoclassical transport show that the electron flutter motion due to the RMP islands introduces a radial particle flux that is not strong enough to directly provide the measured enhancement in the transport, but may contribute to the observed change in the radial electric field due to the ambipolar potential.

1. Introduction

In order to achieve the required confinement for producing significant fusion gain, the high confinement mode (H-mode) is the selected mode of operation in the International Thermonuclear Experimental Reactor (ITER). However, along with the H-mode come edge localized modes (ELMs), or intermittent magnetohydrodynamic (MHD) bursts, that can produce substantial pulses of thermal energy from the plasma edge to the plasma facing components [1], which can drastically decrease divertor lifetimes, generate impurities, and erode first wall components. Resonant magnetic perturbations (RMPs) have been shown to mitigate and/or suppress ELMs in DIII-D [2]-[4] and many other fusion experiments [5]-[8]. A leading hypothesis is that ELM stabilization by RMPs is achieved by significantly increasing the edge plasma transport, preventing the pedestal from reaching the Peeling-Ballooning-Mode (PBM) stability boundary [4], [9].

The observation of spontaneous transitions between ELMing and ELM suppressed conditions with static $n=2$ RMPs reveals that ELM suppression is achieved or lost via a bifurcation in magnetic fields near the inner wall, pedestal impurity toroidal rotation velocity and density fluctuations [10]. Another study using modulated $n = 3$ RMPs in an ELM suppressed state revealed a prompt increase in ion-scale density fluctuations with the increase in the RMP level, indicative of a direct effect of the RMP on turbulence at the pedestal top [3]. Still other studies have revealed increased density fluctuations at intermediate scales at the pedestal top in the transition to ELM suppression [11], [12]. These observations suggest that enhanced top of pedestal turbulent fluctuations may play some roles in the suppression of ELMs, consistent with an earlier hypothesis that enhanced top of pedestal transport is required to suppress ELMs [9].

The effect of the RMP on edge transport changes observed during ELM suppression likely involves a number of factors associated with the resonant and nonresonant effects of the RMP on the plasma. Nonresonant effects are associated with the plasma kink response to the external field and do not involve a topology change in the plasma. Resonant effects involve a change in topology resulting from magnetic island formation and possible magnetic stochasticity when the islands overlap. How these resonant and nonresonant effects influence transport to suppress ELMs has been the subject of extensive research. From first principles global gyrokinetic simulations, using the gyrokinetic toroidal code (GTC) [13,14], it has been demonstrated that the effect of the ideal MHD component of the plasma (kink) response to the RMP has a negligible effect on the linear growth rate of microturbulence and zonal flows at the top of the pedestal, in DIII-D ITER similar shape plasmas for experimentally relevant values of the RMP ($\delta B/B \sim 5 \times 10^{-4}$) [15]. This work suggests that the main nonresonant effect of the RMP on transport is through the neoclassical ambipolar potential or the neoclassical toroidal viscosity (NTV) [16], which can result in changes to the radial electric field (E_r) and its shear.

The effect of magnetic stochasticity on edge transport due to magnetic island overlap has also been explored. However, it is clear from detailed profile measurements on DIII-D that the presence of stochasticity is incommensurate with the inferred electron thermal transport at the top of the pedestal [17]. Therefore, any magnetic resonant mechanism that purports to account for enhanced thermal transport at the top of the pedestal must be a property of isolated non-overlapping magnetic islands. Regardless of the dominant mechanism behind the change in the radial electric field, we need to explore how this change can affect thermal and particle transport in the case where there are good (confining) magnetic surfaces between isolated (small) magnetic islands.

A comprehensive assessment of prompt fluctuation and ExB shear changes in the transition to ELM suppression is beyond the scope of this paper. Therefore, we only confine our present study to the analysis of $n = 2$ RMP ELM suppressed plasmas in the ITER similar shape on DIII-D with static $n = 2$ RMPs, where a concomitant reduction in the ExB shear is seen with the increase in the turbulent fluctuations at the pedestal top in the transition to ELM suppression. In this paper, we show that there is a plausible mechanism to account for the increase in ion-scale turbulence and transport at the top of the pedestal during RMP induced ELM suppression, resulting from the modification of the E_r profile due to $n = 2$ RMPs in the DIII-D tokamak. The mechanism involves a flattening of the E_r profile at the pedestal top, thereby significantly reducing the local ExB shearing rate. Indeed, Fig. 3(c) in [10] shows a strong flattening of the E_r profile (and hence reduction of the ExB shear) at the pedestal top ($\psi_N \sim 0.92$) in the transition to ELM suppression. However, demonstrating the physics mechanism behind the E_r profile change during ELM suppression (i.e., the causality between E_r profile change and ELM suppression) is beyond the scope of this work.

Finally, we cannot claim that the reduction of ExB shear is the cause of the turbulence increase in all cases of RMP ELM suppression. A recent study of ELM suppression with $n = 3$ RMP reveals no significant increase in the top of pedestal ion scale fluctuations, nor a significant decrease in the ExB shear in the transition to ELM suppression (see Fig. 13 in [12]). Another study using modulated $n = 3$ RMPs in an ELM suppressed state indicated that an increase in ion-scale turbulence with increasing RMP level before an observable change in the ExB shear [3]. We also note that an increase in fluctuations at intermediate scales ($k\rho_s > 2$) is seen during $n = 2$ and $n = 3$ ELM suppression [11], [12]. These various studies performed under different plasma conditions and with different RMP fields yield a somewhat confusing array of results. These results indicate that a comprehensive assessment of the conditions in ELM suppression over a wide range of conditions is needed.

2. Simulations of microturbulence in DIII-D pedestal top

Here we use as input to GTC the equilibrium profiles obtained from $n = 2$ ELM suppression studies reported in [10]. In [10], a concomitant flattening of the ExB shear and increase in ion-scale fluctuations is seen at the top of the pedestal in the ELM suppressed state compared to ELMing conditions with the same level of RMP. Similarly, a reduction in turbulence and transport is seen in the transition from ELM suppression to ELMing conditions. The reduction in the fluctuations is correlated with an increase in the top of pedestal ExB shear. Here we analyze three kinetic equilibria generated from the data collected in the $n = 2$ RMP experiment. The first, for discharge #158104 is taken at $t=1350$ ms during the ELMing phase before the $n = 2$ RMP is turned on. The second and third equilibria are from discharge #158103 during $n = 2$ RMP ELM suppression at $t=3050$ ms and during ELMing conditions with RMP at $t=3750$ ms, respectively. A description of the plasma conditions can be found in [10] and a description of the $n = 2$ RMP field amplitude and spectrum can be found in [15].

Figure 1 shows the profiles for these three sets of DIII-D equilibria. By comparing the scale length profiles, we see that the ELM suppressed case has lower R_0/L_n and R_0/L_T at the pedestal top ($\psi_N \sim 0.94$), when compared to the ELMing cases. In the absence of ExB shear, these profile changes will tend to reduce the drive for ion scale turbulence in ELM suppression, relative to ELMing conditions. However, using GTC simulations, we show that the reduction in the ExB shear during ELM suppression (shown in figure 1(e)) leads to an overall increase in the top of pedestal ion scale turbulence, consistent with experiment.

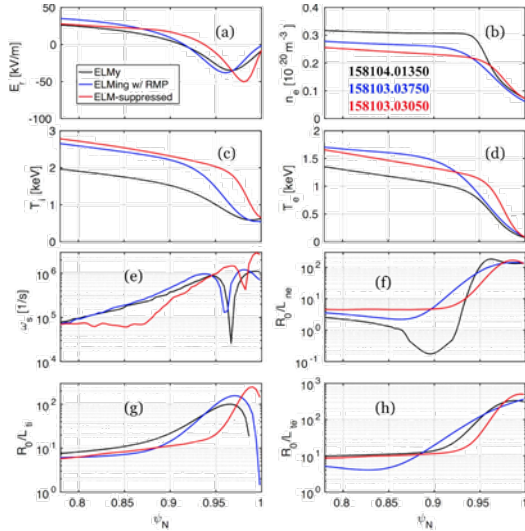


Figure 1. Equilibrium plasma profiles from DIII-D shot 158104 @ 01350 ms (ELMing case before RMP, black), 158103 @ 03750 ms (ELMing with RMP, blue), and 158103 @ 03050 ms (RMP ELM suppressed, red) [10]. (a) Equilibrium radial electric field. (b) Electron density. (c) Ion temperature. (d) Electron Temperature. (e) E_r shearing rate ω_s . (f) Electron density scale length. (g) Ion temperature scale length. (h) Electron temperature scale length. The pedestal top region corresponds to $\psi_N = [0.9, 0.95]$.

In the following simulations, numerical convergence has been obtained. The number of particles per cell, for both ions and electrons, is 100 or 10 for nonlinear or linear simulations, respectively. The time step used is $\Delta t C_S/R_0 = 0.008$. The spatial resolution is $\Delta\rho/\rho_i \sim r\Delta\theta/\rho_i \sim 0.25$, and there are 32 poloidal cross-sections in the whole torus. The radial domains used are $\psi_N = [0.67, 0.97]$ for 158104.01350 and 158103.03750, and $\psi_N = [0.68, 0.98]$ for 158103.03050, where ψ_N is the normalized poloidal flux. The perturbed electric field is solved with a Dirichlet boundary condition, and neither

toroidal nor poloidal filtering is performed on the solution. Profiles are measured using active carbon charge exchange spectroscopy and Thomson scattering measurements, as described in [10], and 3D magnetic equilibria are obtained from VMEC [14]. Since the effects of 3D magnetic perturbation with closed flux surface on the pedestal top turbulence [15] was found to be small in earlier GTC simulations, only the axisymmetric $n = 0$ equilibrium profiles are kept in this work, so as to focus our study on the effects of the profile differences between ELMing and ELM suppressed plasmas. When using collisions we use the electron-ion Lorentz scattering model and in this case $v_{e,i} \sim v_{e,e} \gg v_{i,i}$, with $v^* = v_{e,i}/\omega_{b,e} = 0.031$, where $\omega_{b,e}$ is the electron bounce frequency.

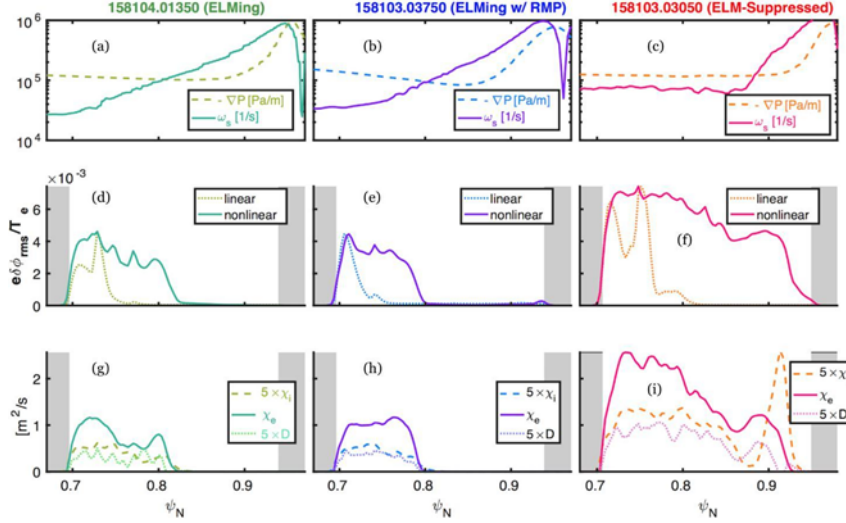


Figure 2. Radial plasma profiles and results from GTC simulations of three DIII-D equilibria for (top row) pressure drive and E_r shearing rate, (middle row) flux-surface-averaged fluctuation amplitudes in linear and nonlinear phases, and (Bottom row) transport coefficients for ion and electron heat conductivities, and particle diffusivity. All physical units are in SI units.

Nonlinear simulations with both collisions and E_r for all three DIII-D cases of 158104.01350, 158103.03750, and 158103.03050 are carried out. Figure 2 depicts the radial profiles of simulation inputs and simulation results in both linear and nonlinear phases. The figure shows the pressure drive and E_r shear profiles (top row), radial profiles for the linear and nonlinear phases of the fluctuation amplitudes (middle row), and the calculated transport coefficients (bottom row). In all three cases, linear eigenmodes are localized away from the pedestal top $\psi_N = [0.7, 0.8]$, with those of 158103.03050 (during ELM suppression) being slightly broader. Nonlinear spreading of turbulence is observed in all three cases, however, the larger ExB shearing rate at the top of the pedestal in the ELMing cases prevents the turbulence from spreading past $\psi_N \sim 0.8$. In the ELM suppressed case, the ExB shearing rate is significantly lower between $\psi_N = [0.8, 0.9]$, and the turbulence is observed to spread to the pedestal top at $\psi_N = 0.93$. Similar trends are found in the heat and particle transport coefficient, shown in figure 2(g-i). The weakened ExB shear in the ELM suppressed case leads to higher transport coefficients at the top of the pedestal relative to the ELMing cases. These results show that the RMP-induced E_r changes can enhance microturbulence near the pedestal top, which is consistent with experimental observations [10] of increased ion-scale turbulence and transport near the pedestal top during RMP induced ELM suppression.

The 2D poloidal mode structures for the linear and nonlinear simulations for these three cases, are shown in figure 3. The upper row depicts the linear phases, which show ITG-like modes. The black dashed lines depict the simulation boundaries, and the red curves show the $q=4$ surface in each case. The

lower row presents the nonlinear phases of the GTC simulations. It can be seen that the microturbulence spreads to the $q=4$ surface only for the ELM suppressed case, and not for the two ELMing cases. The turbulence is shown to spread farther in figure 3(f) than figure 2(f), as in the former we perform rms averages over poloidal angle, and in the latter the outer mid-plane is shown.

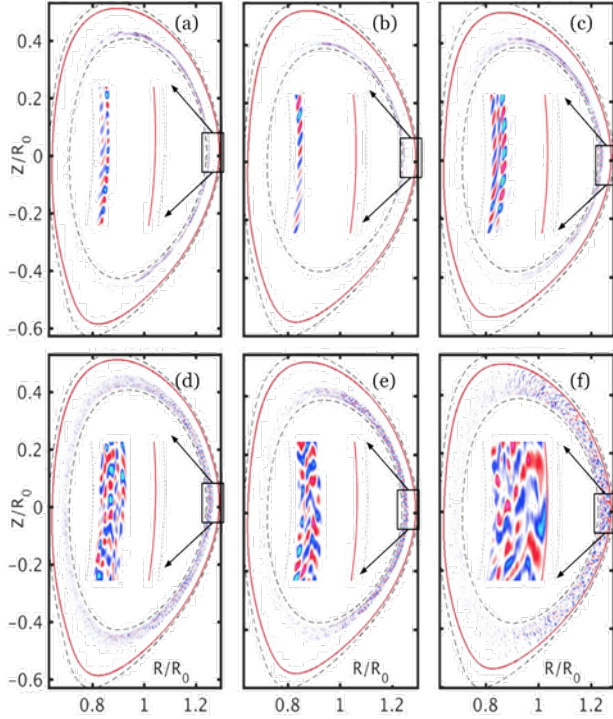


Figure 3. 2D poloidal cross sections of linear (upper row) and nonlinear (lower row) phases of electrostatic fluctuations from GTC simulations of three DIII-D equilibria. Black dashed lines define simulation boundaries, and red solid lines mark the location of the $q=4$ surface. Detailed mode structures near outer mid-plane are shown in the blowups.

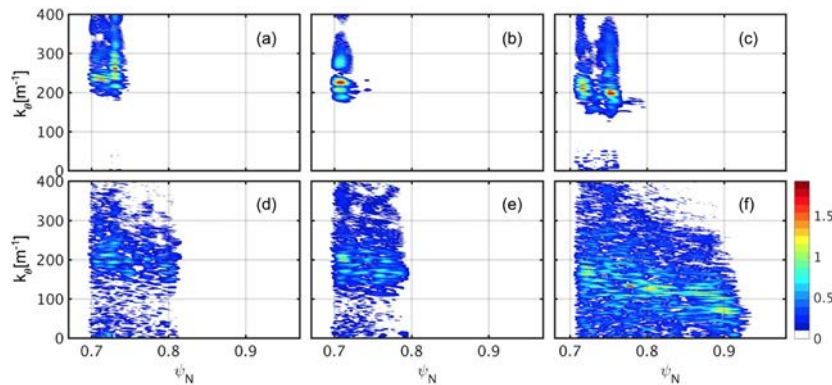


Figure 4. Poloidal wavenumbers of fluctuation spectra of linear (a - c) and nonlinear (d-f) phases of electrostatic fluctuations from GTC simulations of DIII-D shots 158104.01350 (ELMing, first column), 158103.03750 (ELMing with RMP, second column), and 158103.03050 (ELM-suppressed via RMPs, third column). Nonlinear magnitudes are given on the same scale for comparison, while linear magnitudes are arbitrary and simply indicate the dominant radial and spectral locations.

Figure 4 shows the linear and nonlinear spectra of poloidal wavenumber for these three cases. It can be seen that there is significant outward spreading of the longer wavelength turbulence in the ELM suppressed case, as the turbulence is observed to spread to the pedestal top, $\psi_N=0.93$ in that case only. The ELMing cases, with and without $n = 2$ RMPs, do not exhibit a strong downward spectral cascade, nor outward spreading, as there is a large ω_s separating the regions of significant linear instability and the pedestal top.

Summary-- Nonlinear electrostatic GTC simulations of DIII-D shot 158104 at 1350 ms (ELMing no RMP), 158103 at 3750ms (ELMing with $n = 2$ RMP), and 158103 at 3050 ms (ELM suppressed with $n = 2$ RMP) find significantly larger and broader turbulence and transport at the pedestal top in the ELM suppressed case. From gyrokinetic simulations, linear eigenmodes, localized in the core, nonlinearly spread to the pedestal top. This increase in turbulence spreading is attributed to the E_r shearing rate being significantly lower just inside of the pedestal top in the ELM suppressed case. These results are consistent with previous observations [10] of significant increases of fluctuations near the pedestal top, and may explain these observations.

3. Effects of RMP-induced magnetic islands on turbulent and neoclassical transport

Full plasma responses to RMPs, including both kink and tearing parts as provided by the resistive MHD code M3D-C1, have been implemented into GTC to study the effect of magnetic islands and stochastic field regions on microturbulence and neoclassical transport. Electrostatic turbulence simulations with adiabatic electrons show no significant increase of the saturated ion heat conductivity in the presence of RMP-induced islands. However, electron response to zonal flow in the presence of magnetic islands and stochastic fields can drastically increase zonal flow dielectric constant for long wavelength fluctuations. Zonal flow generation can then be reduced and the microturbulence can be enhanced greatly. Finally, neoclassical transport simulations show that the electron flutter motion due to the existence of RMP islands introduces a radial particle flux that is at the same level as the neoclassical electron flux. This flux is not strong enough to directly provide the measured enhancement in the transport, but may contribute to the observed change in the radial electric field. Because the RMP magnetic island size is comparable to the ion banana width, electron and ion responses to these islands may be fundamentally different, which could drive non-ambipolar particles fluxes leading to changes of the radial electric field shear.

4. GTC simulations of microturbulence in stellarator

Fully 3D equilibria have been recently enabled in GTC via an interface with the MHD equilibrium code VMEC. Simulations have been carried out in both full torus and partial torus taking into account the toroidal periodicity of the stellarators. The effects of toroidal mode coupling on linear dispersions and mode structures in Wendelstein7-X (W7-X) and Large Helical Device (LHD) stellarators are studied. The linear growth rates, real frequencies, and mode structures agree reasonably well with the results obtained by the EUTERPE code. The partial torus simulation, although restricted by the machine periodicity, successfully captures the main ballooning feature of the eigenmode.

Acknowledgements. This work is supported by General Atomics subcontract 4500063485, U.S. DOE theory grant DE-SC0013804 and DE-FG02-07ER54916, General Atomics collaboration agreement under DOE grant DE-FG03-94ER54271, U.S. DOE grant to the Princeton Plasma Physics Lab., award No. DE-AC02-09CH11466, and U.S. DOE SciDAC ISEP center.

Disclaimer: This report was prepared as an account of work sponsored by an agency of the United States Government. Neither the United States Government nor any agency thereof, nor any of their employees, makes any warranty, express or implied, or assumes any legal liability or responsibility for the accuracy, completeness, or usefulness of any information, apparatus, product, or process disclosed, or represents that its use would not infringe privately owned rights. Reference herein to any specific commercial product, process, or service by trade name, trademark, manufacturer, or otherwise does not necessarily constitute or imply its endorsement, recommendation, or favoring by the United States Government or any agency thereof. The views and opinions of authors expressed herein do not necessarily state or reflect those of the United States Government or any agency thereof.

References:

- [1] P. Lang, A. Loarte, G. Saibene, L. Baylor, M. Becoulet, M. Cavinato, S. Clement-Lorenzo, E. Daly, T. Evans, M. Fenstermacher, et al., "ELM control strategies and tools: Status and potential for ITER," *Nuclear Fusion*, vol. 53, no. 4, p. 043 004, 2013.
- [2] T. Evans, R. Moyer, J. Watkins, P. Thomas, T. Osborne, J. Boedo, M. Fenstermacher, K. Finken, R. Groebner, M. Groth, et al., "Suppression of large edge localized modes in high confinement DIII-D plasmas with a stochastic magnetic boundary," *Journal of nuclear materials*, vol. 337, pp. 691-696, 2005.
- [3] G. McKee, Z. Yan, C. Holland, R. Buttery, T. Evans, R. Moyer, S. Mordijck, R. Nazikian, T. Rhodes, O. Schmitz, et al., "Increase of turbulence and transport with resonant magnetic perturbations in ELM-suppressed plasmas on DIII-D," *Nuclear Fusion*, vol. 53, no. 11, p. 113011, 2013.
- [4] M. Wade, R. Nazikian, T. Evans, N. Ferraro, R. Moyer, D. Orlov, R. Buttery, M. Fenstermacher, A. Garofalo, M. Lanctot, et al., "Advances in the physics understanding of elm suppression using resonant magnetic perturbations in DIII-D," *Nuclear Fusion*, vol. 55, no. 2, p. 023002, 2015.
- [5] Y. Liang, H. Koslowski, P. Thomas, E. Nardon, B. Alper, P. Andrew, Y. Andrew, G. Arnoux, Y. Baranov, M. Becoulet, et al., "Active control of type-I edge-localized modes with $n=1$ perturbation fields in the jet tokamak," *Physical review letters*, vol. 98, no. 26, p. 265004, 2007.
- [6] A. U. Team, W. Suttrop, T. Eich, J. Fuchs, S. Gunter, A. Janzer, A. Herrmann, A. Kallenbach, P. Lang, T. Lunt, et al., "First observation of edge localized modes mitigation with resonant and nonresonant magnetic perturbations in ASDEX upgrade," *Physical Review Letters*, vol. 106, no. 22, p. 225004, 2011.
- [7] Y. Jeon, J.-K. Park, S. Yoon, W. Ko, S. Lee, K. Lee, G. Yun, Y. Nam, W. Kim, J.-G. Kwak, et al., "Suppression of edge localized modes in high-confinement KSTAR plasmas by nonaxisymmetric magnetic perturbations," *Physical review letters*, vol. 109, no. 3, p. 035004, 2012.
- [8] A. Kirk, Y. Liu, E. Nardon, P. Tamain, P. Cahyna, I. Chapman, P. Denner, H. Meyer, S. Mordijck, D. Temple, et al., "Magnetic perturbation experiments on MAST I-and H-mode plasmas using internal coils," *Plasma Physics and Controlled Fusion*, vol. 53, no. 6, p. 065011, 2011.

- [9] P. Snyder, T. Osborne, K. Burrell, J. Candy, R. Groebner, A. Leonard, R. Nazikian, D. Orlov, O. Schmitz, M. Wade, et al., "The EPED pedestal model: Extensions, application to ELM-suppressed regimes, and ITER predictions," in Proceedings of the 24th IAEA Fusion Energy Conf., San Diego, California, 2012.
- [10] R. Nazikian, C. Paz-Soldan, J. Callen, D. Eldon, T. Evans, N. Ferraro, B. Grierson, R. Groebner, S. Haskey, C. Hegna, et al., "Pedestal bifurcation and resonant field penetration at the threshold of edge-localized mode suppression in the DIII-D tokamak," Physical review letters, vol. 114, no. 10, p. 105002, 2015.
- [11] C. Paz-Soldan, R. Nazikian, R. Moyer, J. Callen, et al., "Optimization of the plasma response for the control of edge-localized modes with 3D fields," in Proceedings of the 26th IAEA Fusion Energy Conf., Kyoto, Japan, 2016.
- [12] R. A. Moyer, C. Paz-Soldan, R. Nazikian, D. M. Orlov, N. Ferraro, B. A. Grierson, M. Knolker, B. Lyons, G. R. McKee, T. H. Osborne, et al., "Validation of the model for ELM suppression with 3D magnetic fields using low torque ITER baseline scenario discharges in DIII-D," Physics of Plasmas, vol. 24, no. 10, p. 102501, 2017.
- [13] Z. Lin, T. S. Hahm, W. Lee, W. M. Tang, and R. B. White, "Turbulent transport reduction by zonal flows: Massively parallel simulations," Science, vol. 281, no. 5384, pp. 1835-1837, 1998.
- [14] Y. Xiao, I. Holod, Z. Wang, Z. Lin, and T. Zhang, "Gyrokinetic particle simulation of microturbulence for general magnetic geometry and experimental profiles," Physics of Plasmas, vol. 22, no. 2, p. 022516, 2015.
- [15] I. Holod, Z. Lin, S. Taimourzadeh, R. Nazikian, D. Spong, and A. Wingen, "Effect of resonant magnetic perturbations on microturbulence in diiii-d pedestal," Nuclear Fusion, vol. 57, no. 1, p. 016005, 2016.
- [16] W. Zhu, S. Sabbagh, R. Bell, J. Bialek, M. Bell, B. LeBlanc, S. Kaye, F. Levinton, J. Menard, K.-C. Shaing, et al., "Observation of plasma toroidal-momentum dissipation by neoclassical toroidal viscosity," Physical review letters, vol. 96, no. 22, p. 225002, 2006.
- [17] I. Joseph, "Edge-localized mode control and transport generated by externally applied magnetic perturbations," Contributions to Plasma Physics, vol. 52, no. 5-6, pp. 326-347, 2012.